MINERALOGICAL INVESTIGATION OF POSSIBLE IMPACT MELT POOL OF THE MOON's SOUTH POLE-AITKEN BASIN. M. Ohtake[1], K. Uemoto[2], J. Haruyama[1], R. Nakamura[3], T. Matsunaga[4], S. Yamamoto[4], Y. Yokota[5], Y. Ishihara[1], T. Iwata[1]. [1]Japan Aerospace Exploration Agency(JAXA) (ohtake.makiko@jaxa.jp), [2]Tokyo Univ., [3]National Institute of Advanced Industrial Science and Technology, [4]National Institute for Environmental Studies, [5]Tsukuba Planetary Study Group.

Introduction: The South Pole-Aitken (SPA) basin is the largest basin that is clearly identified on the Moon. It was determined to have an elliptical structure with a 2400 km major axis and a 2050 km minor axis in a recent study [1]. The basin impact is very large, so it has been suggested that most of the crustal material within the SPA was excavated [2], and it is likely that the mantle materials have been exposed within the basin. However, the mineralogy of the SPA basin was not well known previously because it is one of the oldest basins (pre-Nectarian in age [3]), and its surface has become obscured by intensive cratering and mixing since its formation. Therefore, we conducted a detailed mineralogical investigation within the SPA basin and found a possible impact melt pool at the center of the basin (162.6°E, 53.7°S, 315 and 343 km radius) [4]. However, the materials in the center of the basin should have melted [e.g., 3]. A recent study reported that the impact melt generated by the SPA basin impact and the mantle material melted to about a 700 km depth [5, 6], and that the final depth of the impact melt after basin transition was about 50 km [7]. Therefore, it is very important to investigate the mineralogy and composition of the impact melt pool and to evaluate if the impact melt pool had undergone magmatic differentiation to acquire rare direct information of the lunar mantle composition.

In this study, we used a new mineralogical map based on high-spatial-resolution reflectance spectra using the SELENE (Kaguya) Multiband Imager (MI) [8] to address these issues. We investigated not only the mineralogy but also the layer thickness, distributions, chemical abundance, and stratigraphy within the central area of the basin. We then compared our observations to the available estimation of the lunar mantle composition and magmatic differentiation studies [9].

Methods: Seven thousand Kaguya MI map data files [8] with a spatial resolution of 14 m/pixel were used to generate a binned low-resolution MI reflectance map (237 m/pixel) within the center of the SPA basin (around the central depression from [4], at 40 to 70°S and 140 to 220°W). The wavelength assignment of MI provides both visible and near-infrared coverage in spectral bands of 415, 750, 900, 950, 1000, 1050, 1250, and 1550 nm. Mineral phases have diagnostic absorption features in this wavelength range, depending on the mineral phases and their compositions. We made a color-composite image from these data (RGB map). The colors were assigned to continuum-removed absorption depths to generate these images: red for 900 nm (low-Ca pyroxene; LCP), green for 1050 nm (olivine or high-Ca pyroxene; HCP), and blue for 1250 nm (plagioclase). In addition, we made iron (FeO) and titanium (TiO_2) abundance maps using the Lucey method [10] on the MI data [11] and generated a geological map and geologic columnar section of the area. The thickness of each rock type layer was estimated by observing the composition of the crater wall and floor of variable size (300 craters from 2 to 75 km in diameter) and using the relation between the crater diameter and excavation depth.

Results: We classified the rock types for six units (orange, cyan, yellow, white, brown, and blue). Orange represents the LCP-dominant unit (L1) located around the central depression, which was also exposed a little in the central depression. Cyan represents the HCP-dominant unit (H1) located within the depression, which is mostly located in the eastern half of the depression. Yellow represents an HCP-dominant unit (H2) with relatively deeper spectral absorption at 1050 nm than the 950 and 1000 nm and tends to have longer wavelengths in the band center (about 970 nm) than the cyan unit. The brown layer is an LCP-dominant unit (L2) observed at the central peaks of the large craters, which formed after the SPA basin impact. White represents the HCP-dominant unit (MB) having even longer wavelengths in the band center and higher iron content than the yellow and the brown units and is located within and around relatively large craters. The white unit corresponds to the mare basalt reported in previous works [12]. The blue layer is plagioclase dominant rock (An).

Figures 1a) and b) are a 750 nm band image and rock-type map of the studied area. HCP-dominant rock types (H1 and H2) have the largest coverage in the central depression. Based on the crater wall and floor observation on the L1 unit, it is clear that the H1 unit extends under the L1 unit. The L1 thickness is estimated to be 100 to 500 m based on the estimated excavation depth of the observed craters (Fig. 2a). Based on the crater central peak observation of the H1 unit, the LCP-dominant L2 unit underlays the H1 unit, and the H1 thickness is from 6.5 to 6.9 km (Fig. 2b). Similarly, H1 extends under the H2 unit and is up to 2 km thick, although the value varies with the location. The thickness of the brown unit could not be estimated because

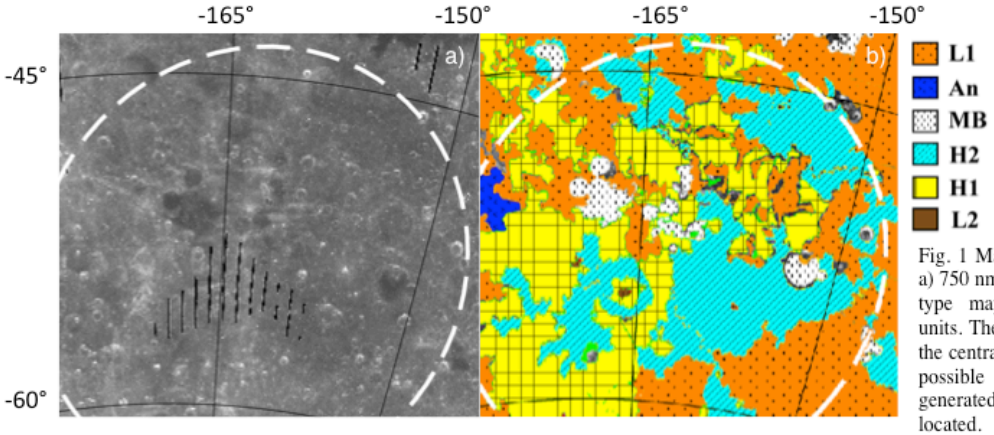

Fig. 1 Map of the studied area. a) 750 nm band image. b) Rock-type map classified into six units. The white circle indicates the central depression where the possible impact melt pool generated by the SPA impact is located. Rock types are described in the text.

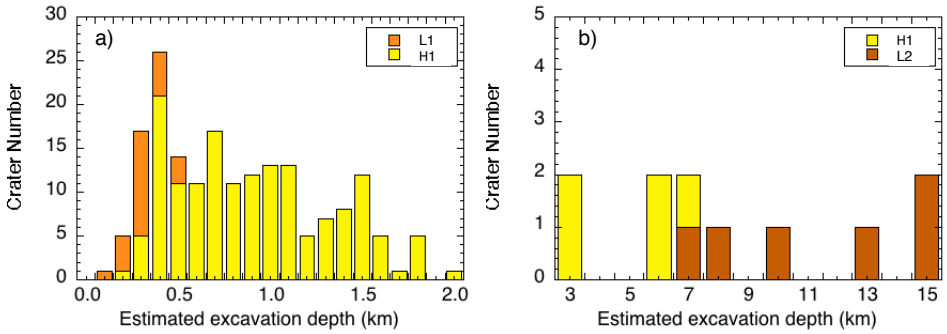

Fig. 2 Number-excavation depth histogram of the rock types exposed in craters. a) Small scale up to 2 km. b) Large scale from 3 to 15 km.

there is no crater or central peak to expose the lower portion of the red layer. However, it is at least 8 km thick, based on the diameters of the smallest and largest craters that have central peaks of the red layer. As a result, columnar sections of the area are determined as L2> H1> (L1/H2) from bottom to top.

We interpreted the L1 unit as mantle material ejected by an SPA formed impact event based on its spectra, thickness, and chemical composition. We also interpreted the H1 and L2 units as the impact melt of the SPA basin that had undergone magmatic differentiation. There are multiple reasons for this interpretation. This layer is larger and thicker than the normal mare basalt observed on the Moon (the maximum thickness was estimated at 2.0 to 5.2 km even in the Imbrium basin, the largest basin on the Moon, where mare basalt covers the entire basin area [13, 14]). In addition, the average FeO abundance is 2 wt.% lower than that of mare basalt. For these reasons, it is likely that this layer is not mare basalt but is impact melt that pooled during formation of the SPA and differentiated. We interpreted the An unit as exposed material of an inner edge of the excavated crust by SPA basin generated impact.

Discussion: Reference [9] studies SPA impact melt differentiation and derived estimated stratigraphy considering the different lunar bulk composition (different impact melt composition) and mantle overturn. Stratigraphy of our observation (lower LCP layer of at least 8 km and upper HCP layer of 6~7 km) is matched to the stratigraphy of a post-overturn model in their study, which estimated relatively thick olivine layer (~30 km)> LCP layer (12 km)> HCP layer (5 km) from bottom to top in the differentiated column. This suggest that the composition of the SPA impact melt indicates the lunar upper mantle after the mantle overturn. In other words, the SPA impact event occurred after the LMO cumulate overturn. This is possibly direct evidence that the mantle overturn occurred early in the history of the Moon.

References: [1] Garrick-Bethell and Zuber (2009) *Icarus*, 204, 399–408. [2] Spudis et al. (1994) *Science*, 266, 1848-1851. [3] Melosh. (1989), Impact Cratering: A Geologic Process, Oxford Univ.Press, London. [4] Ohtake et al. (2014) *GRL*, 41, 2738–2745. [5] Lucey et al. (1998) *JGR*, 103, NO. E2, 3701-3708. [6] Potter et al. (2012) *Icarus*, 220, 730–743. [7] Vaughan et al. (2014) *PSS*, 91, 101-106. [8] Ohtake et al. (2008) *EPS,* 60, 257–264. [9] Hurwitz and Kring (2014) *JGR*, 119, 1110–1133. [10] Lucey et al. (2000) *JGR,* 105, 20,297-20,305. [11] Otake et al. (2012) *LPSC*,1905. [12] Pieters et al. (2001), *JGR*, 106, E11, 28,001-28,022. [13] Williams and Zuber (1998) *Icarus,* 131, 107–122. [14] Thomson et al. (2009) 36, L12201.